Rate and Mechanisms for Water Exchange around Li^+(aq) from MD Simulations

Daniel Spångberg,[†] Rossend Rey,[‡] James T. Hynes,[§,||] and Kersti Hermansson*,[†]

Materials Chemistry, The Ångström Laboratory, Uppsala University, Box 538, S-751 21 Uppsala, Sweden, Departement de Física i Enginyeria Nuclear, Universitat Politècnica de Catalunya, Campus Nord B4-B5, Barcelona 08034, Spain, Département de Chimie, UMR 8640 PASTEUR, Ecole Normale Supérieure, 24, rue Lhomond, 75231 Paris, France, and Department of Chemistry and Biochemistry, University of Colorado, Boulder, Colorado 80309-0215

Received: October 17, 2002; In Final Form: February 3, 2003

The solvent exchange rate of aqueous Li^+ has been determined by employing the reactive flux method in combination with very long molecular dynamics simulations based on effective three-body ion−water potentials. The mechanisms for the resulting exchange events have been studied in considerable detail and analyzed in terms of the five commonly discussed exchange classes: associative (A), dissociative (D), and interchange (I, I_a, I_d). Furthermore, the stereochemistry (cis, trans) of each exchange has been monitored and correlated with the exchange classes. Most of the exchanges are associative or associative interchanges and of a trans type, although the trans exchanges are less probable on a purely statistical basis.

1. Introduction

The exchange of solvent molecules around ions is a topic that has received much attention over the years; see, for example, refs 1−3. In this paper, we present a molecular dynamics computational study of the rate and mechanisms for water exchange for the Li^+(aq) ion. The lithium ion is of special fundamental interest because it is the smallest monopositive ion.

Although there have been various quantum chemical and computer simulation studies of metal ions in water,[4−36] few of these have been concerned with solvent exchange[4−19] and even fewer with the mechanisms of solvent exchange.[4−11] The rate and mechanism of a solvent-exchange process are difficult to obtain from experiment because the reactant and product are the same. Also, the solvent is the same as the entering and leaving groups.[37] Computer simulation can provide a valuable route to examine these issues.

The majority of earlier simulation studies has primarily been concerned with the structure and thermodynamics of ion solvation.[20−34] In studies where the exchange dynamics has been examined, the discussion has focused on the residence times and exchange rates of solvent molecules in the first solvation shell of the ions,[12−19] with detailed mechanisms being examined only in refs 4−7.

As far as Li^+(aq) is concerned, literature data give average coordination numbers varying between 3.7 and 6.1 (Table 1). However, more recent results favor the smaller coordination number. In general, simulation studies of metal ions in aqueous solution where many-body effects are included (implicitly or explicitly) tend to give a lower coordination number.[15,30,32−34]

The average residence time of a water molecule in the first hydration shell of Li^+(aq) has been determined by quasi-elastic neutron scattering[38] (QENS) to be less than 100 ps. Simulation studies in the literature give residence times between 25 and 400 ps (Table 2). This relatively large discrepancy is likely related to the limited number of exchange events observed and also to the fact that the energy difference between the differently coordinated species is small.[35] Thus, a small change in the ion−water and/or water−water potential changes the probability of finding an ion with different coordination.

As far as mechanisms for the exchange of ligands around ions are concerned, Langford and Gray proposed a scheme[39] in which a mechanism is defined as associative (A) if a two-step path involving an intermediate of a higher coordination number can be detected and dissociative (D) if a lower coordination number can be detected. If no such intermediate can be found, then the mechanism is termed interchange (I), which is subdivided into two classes (I_a, I_d) depending on whether the exchange is associative-like or dissociative-like. This scheme can be correlated[39] with the scheme of Basolo and Pearson[40] that in turn is based on the Hughes−Ingold scheme,[41] originally introduced for organic substitution reactions. The A mechanism corresponds to the S_N2 (lim) reaction, the I_a mechanism, to the S_N2 reaction, and the D mechanism, to the S_N1 (lim) reaction whereas the I_d mechanism takes a borderline position, but in the scope of this article, it can be thought of as S_N1. The scheme proposed by Langford and Gray was later extended by Merbach et al.,[2,42,43] who emphasize a structural definition of the exchange depending on the degree of contraction or expansion of the hydration shell during the exchange, making use of the same notation but including a set of five classes (A, I_a, I, I_d, and D). The five exchange classes are illustrated schematically in Figure 1 and are adopted in the present work.

Basolo and Pearson[40] discuss the stereochemistry of ligand-substitution mechanisms in terms of trans and cis attacks, depending on the position of the entering ligand relative to the leaving ligand. Kowall et al.[5] found from MD simulations that the I_d exchanges around Nd^{3+}(aq) and the I_a exchanges around Yb^{3+}(aq) take the least sterically hindered path, corresponding to trans exchanges around tetrahedral and octahedral complexes. Rotzinger[10] found from ab initio cluster calculations that both cis and trans substitutions are possible for the concerted (interchange) mechanism in the middle of the transition-metal series.

The continuous development of computers is beginning to make it feasible to study the structure and dynamics of quite

* To whom correspondence should be adressed. E-mail: kersti@mkem.uu.se.
[†] Uppsala University.
[‡] Universitat Politècnica de Catalunya.
[§] Ecole Normale Supérieure.
[||] University of Colorado.

10.1021/jp027230f CCC: $25.00
Published on Web 04/11/2003

TABLE 1: Theoretical and Experimental Literature Data for Li−O Distances and Coordination Numbers in Li^+(aq) Solutions

method	Li−O distance (Å)	coordination number	concentration	counterion
MD (this work)	1.96	4.02	1::512	none
ab initio MD[11]	1.96	4	1::32	none
QM/MM[34]	1.94	4.1	1::199	none
MD[27]	1.90	4	1::460[a]	none
MD[7]	2.07	6.0	1:1:123	Cl^-
MD[19]	1.95	4.1	1::215	none
MD[26]	1.90 ± 0.05	4	1::—[a]	none
MD[16]	2.0	4.5	1::525	none
MD[18]	1.95	4.1	1::215	none
thermodynamic cycle[25]		4		
ab initio[35,36]	1.916−2.009	4		
MD[17]	2.20	6.0	1::215	none
MC[23]	1.96	4.0	1::125	none
RISM[29]	1.90	3.7		none
MD[28]	2.04	6.0	1::64	none
MD[22]	2.00	5.2	36:36:198	Cl^-
MD[12]	1.98	5.3	1::64	none
MD[21]	2.12	6.1	8:8:200	I^-
MD[20]	2.15	5.5	9:9:198	Cl^-
neutron diffraction[63]	1.94	4.5 ± 0.5	1.88 M	Br^-
X-ray diffraction[64]	1.99−2.07	4	2.29−5.24 M[b]	Cl^-[b]
neutron diffraction[65]	1.95 ± 0.02	5.5 ± 0.3,[c] 3.3 ± 0.5[d]	3.57 m, 9.95 m	Cl^-

[a] Ion fixed at the center of a sphere of water molecules. [b] Concentration of Li^+. $CoCl_2$−LiCl aqueous solution. [c] Concentration 3.57 *m*. [d] Concentration 9.95 *m*.

TABLE 2: Theoretical and Experimental Literature Data for Mean Residence Times

method	residence time (ps)
MD (this work)	112 ± 16[a]
ab initio MD[11]	20−50
MD[7]	300[b]
MD[19]	50.6
MD[18]	400
MD[16]	41.4
MD[17]	184
MD[12]	33.3
MD[13]	25 ± 5
QENS[38]	≤100

[a] Value from reactive flux calculations. [b] One single exchange in 300 ps.

large systems using ab initio methods. Feller et al.[35,36] performed calculations on $Li(H_2O)_n$ clusters for $n = 1-6$ using extended basis sets and various correlation methods with up to MP2 for the larger clusters. For a set of optimized $Li(H_2O)_6$ clusters, the lowest-energy cluster had four water molecules bound to the ion and two in the "second solvation shell". The structure of Li^+(aq) has been studied by Tongraar et al.[34] using a Born−Oppenheimer QM/MM ab initio dynamics method on a lithium ion solvated in 199 water molecules, where the first solvation shell was treated at the HF/LANL2DZ level and the rest of the system was described with pair potentials; the resulting average coordination number was 4.1. The dynamics has also recently been studied by Lyubartsev et al.,[11] who used the Car−Parrinello approach to simulate 1 Li^+ ion in 32 water molecules. They found that the lithium ion was usually tetrahedrally coordinated, and during the simulation, two associative (or associative interchange) exchanges were found. The residence time for the water molecules in the first hydration shell was estimated to be between 20 and 50 ps. Despite the increasing availability of computing power, many condensed-matter properties require such long simulation times and/or large simulation systems that classical simulations are still virtually indispensable. The study of exchange mechanisms is one such example: in the present study, we could examine approximately 330 exchange events in the most efficient classical simulation sampling.

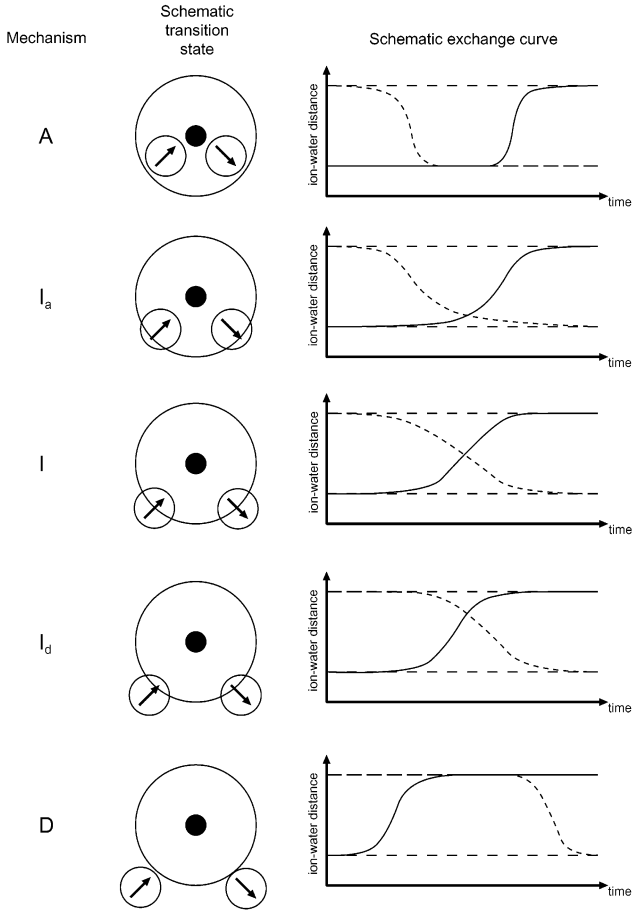

Figure 1. Structural definition of the five exchange classes. First column: classification of exchange mechanism. Second column: schematic illustration of the exchanges according to DuCommun and Merbach.[2] Third column: ion−oxygen distance exchange curves for the ideal exchanges.

Here, a new lithium−water effective three-body potential,[44] consistent with recent experiments and calculations, is used in combination with the method of Rey and Hynes.[14] This allows the determination of the transmission coefficient as well as an

accurate exchange rate constant. Also, the study of a very large number of exchange events is possible. The stereochemistry of each of these exchange events was monitored and correlated with the five exchange classes.

The outline of the remainder of this paper is as follows. In section 2, we describe the methodology for obtaining the rate constant and examining exchange trajectories, with various details of the simulations given in section 3. The results for the rate constant and various mechanistic aspects are discussed in section 4, and our conclusions are given in section 5.

2. Methodology

2.1. Exchange Rate of Water Molecules around Li^+. The exchange rate was here obtained in the manner described by Rey and Hynes.[14] Thus, the dissociation rate constant is written as $k = \kappa k^{TST}$, where k^{TST} is the transition-state rate constant and κ is the transmission coefficient, which is a measure of the fraction of successful exchange events given activated conditions.

The reaction coordinate is here defined as the distance between the ion and the center of mass of the water molecule. The transition-state rate constant can be obtained using[14,45]

$$k^{TST} = \sqrt{\frac{k_B T}{2\pi\mu}} \frac{r^{\ddagger 2} e^{-\beta W(r^\ddagger)}}{\int_0^{r^\ddagger} r^2 e^{-\beta W(r)}} = \sqrt{\frac{k_B T}{2\pi\mu}} \frac{e^{-\beta W_{eff}(r^\ddagger)}}{\int_0^{r^\ddagger} e^{-\beta W_{eff}(r)}} \quad (1)$$

where μ is the ion−water reduced mass, β is equal to $1/k_B T$, $W(r)$ is the potential of mean force (PMF), and $r^\ddagger$ is the distance between the ion and water molecule at activated conditions. $W_{eff}(r)$ is the centrifugally averaged (effective) PMF. For exchanges that are fast on the time scale of the total simulation time, the obtained $g(r)$ is reliable in the area between the first and second hydration shells, and the PMF can be obtained directly from the radial distribution function according to

$$W(r) = -k_B T \ln(g(r)) \quad (2)$$

However, for slower exchanges, the statistical uncertainty of the radial distribution function in the region between the first and second hydration shells (i.e., in the region of exchange) makes it difficult to obtain a reliable potential of mean force. Here, a constraint method used previously for ion pairs[46,47] was employed to obtain a full, reliable PMF.

Thus, the distance between the ion and the water molecule's center of mass was constrained in several steps between the first and second hydration shells (2.3−3.4 Å), and the mean force on the Li^+−water constraints was determined. The PMF was subsequently calculated by integrating the mean force, with the integration constant chosen such that the resulting PMF coincides with the PMF calculated from the radial distribution function according to eq 2.

The transmission coefficient κ was obtained using the method of reactive flux.[14,48,49] The normalized reactive flux can in the present case be computed as

$$k(t) = \frac{\langle \dot{r}(0)\, \theta[r(t) - r^\ddagger] \rangle_c}{\langle \dot{r}(0)\, \theta[\dot{r}(0)] \rangle_c} \quad (3)$$

$\theta[x]$ is the Heaviside step function, which is 1 if x is larger than 0 and 0 otherwise. The averages were computed by starting several trajectories from equilibrated configurations with the Li^+−water center-of-mass distance constrained at $r^\ddagger$, as indicated by the subscript c. The Li^+−water constraints were then removed, new velocities were sampled from a Boltzmann distribution, and the system was allowed to propagate both forward and backward in time. The transmission coefficient κ was then obtained as the plateau value of the normalized reactive flux.

2.2. Alternate Approaches for the Rate Constant. The rate constant can in principle also be computed from the direct simulation trajectories. The average of the residence-time correlation function is defined as follows:[12,14]

$$\langle R(t) \rangle = \left\langle \frac{1}{N} \sum_{i=1}^{N} \theta(r^\ddagger, 0)\, \theta(r^\ddagger, t) \right\rangle \quad (4)$$

The entire function was fitted to an exponential decay function $\langle R(t) \rangle \approx e^{-kt}$ giving the rate constant k. In eq 4, N is the number of water molecules in the first hydration shell at time $t = 0$. When computing the $\theta(r^\ddagger, t)$ function, a tolerance time, $t^* = 2$ ps, for the escape of a water molecule from the first hydration shell was used, which approximately corresponds to the time it takes for a water molecule to diffuse one molecular radius.[12] If a water molecule leaves the first hydration shell but returns before this time, then the water molecule is considered not to have left the first hydration shell at all. The result is not very dependent on the value of the tolerance time as long as it is reasonable.

In the present case, where the cation−water interactions are rather strong and the exchange events are relatively rare (compared to Na^+, for example), it is necessary to perform a very long simulation to obtain good statistics for the direct simulation trajectories. We have here decided to be satisfied with moderately good statistics in the case of the calculation in section 4.2 of the rate constant from direct simulation.

The rate constant was also computed using the Grote−Hynes theory,[50] which gives κ as

$$\kappa_{GH} = \left[\kappa_{GH} + \left(\frac{1}{\omega_b} \right) \int_0^\infty dt\, e^{-\omega_b \kappa_{GH} t} \zeta(t) \right]^{-1} \quad (5)$$

in which ω_b is the frequency of the effective potential barrier ($\omega_b \approx 42.3$ ps^{-1}) and the time-dependent friction $\zeta(t)$, which was computed as in ref 14, corresponds to $r = r^\ddagger$.

2.3. Exchange Mechanisms. The exchange mechanisms from the constraint dynamics simulations (see section 2.1) were examined by concatenating the trajectories forward and backward in time, starting from the same configuration with the Li^+−water center-of-mass distance constrained at $r^\ddagger$. All trajectories where the water molecule was initially (the last configuration in the trajectory going backward in time) outside the first hydration shell and finally (the last configuration in the trajectory going forward in time) inside the first hydration shell were stored. For the stored configurations, the distance between the water molecules and the ion was plotted versus time, the distance at the crossing point, where the distance between the ion and the two molecules (the previously constrained and the "free" one) is the same, was evaluated, and the exchange mechanism was determined. Here, the distance between the water molecules and the ion at the crossing point of the incoming and outgoing molecules during the exchange was used to distinguish between the different exchange classes.[6,7] The ion−water distance in the region between the first and second shells (2.02−4.19, see Figure 2) was thus divided into five equal classes (cf. Figure 1).

When the crossing point was closer to the ion than 2.45 Å, the exchange was considered to be of the A type; when the

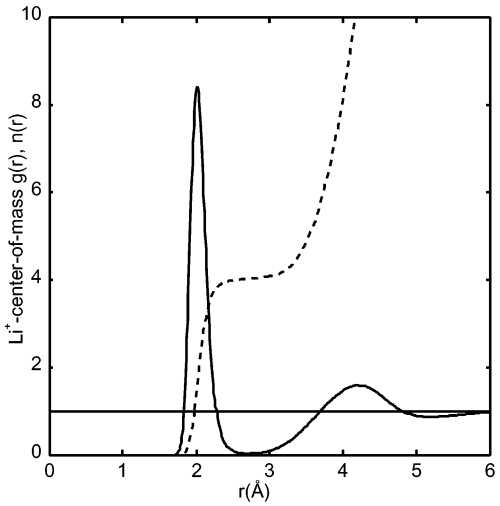

Figure 2. Li^+−water center-of-mass radial distribution function obtained from direct simulation, $g(r)$ (—), and the running integration number, $n(r)$ (- - -).

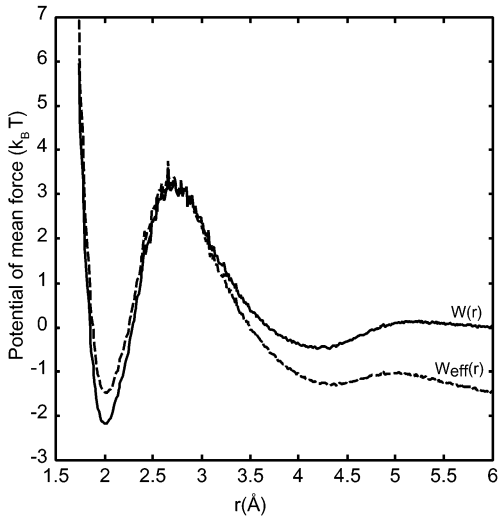

Figure 3. Potential of mean force, $W(r)$, obtained from $g(r)$ (—) and the centrifugally averaged (effective) potential of mean force $W_{eff}(r)$ (- - -)

crossing point was between 2.45 and 2.89 Å, the exchange was considered to be of the I_a type, between 2.89 and 3.32 Å, of the I type, and between 3.32 and 3.76 Å, of the I_d type. Finally, if it was further out than 3.76 Å, it was considered to be of the D type. The stored configurations were also studied with a computer graphics molecular visualization program[51] to determine the stereochemistry of the exchange.

The exchange mechanism from the direct simulation was also studied for comparison. The exchange events were pinpointed by plotting the distances between the ion and all water molecules, whichever came closer than 3 Å to the ion during a 15-ps time interval, versus time. The coordinates for these water molecules were then studied for a short time before and after the exchange event.

3. Simulation Details

Water molecules (512) and 1 lithium ion were placed in a cubic simulation box employing periodic boundary conditions. The water model used was Berendsen's SPC/E water model.[52] The ion−water potential model was an effective three-body potential fitted to ab initio energies.[44] The expression used for the short-range ion−water potential is divided into two parts. One part accounts for the ion−water pair interactions, and the other, for the three-body interactions. The two-body part consists of terms of the following form:

$$U_i = Ae^{-br_i} - \frac{C}{r_i^4} - \frac{D}{r_i^6} \tag{6}$$

r_i is the distance between the ion and the oxygen or hydrogen atoms of the water molecules. The three-body part between the ion and two water molecules is of the form

$$U_{ij} = E(F + \cos(\theta_{ij}))^3 e^{-G(r_i^2+r_j^2)} \tag{7}$$

where i is the oxygen atom of one water molecule and j is the oxygen of the other water molecule. The angle between the first oxygen, the ion, and the second oxygen is represented by θ_{ij}. The distances between the ion and the oxygens of the two water molecules are r_i and r_j. If distances are given in Å and energies in kJ mol^{-1}, then the parameters are as follows: $A_O = 280742.$, $b_O = 4.67052$, $C_O = -972.978$, $D_O = 2681.93$, $A_H = 12569.3$, $b_H = 3.29925$, $C_H = 761.052$, $D_H = -436.749$, $E = 1.15882$, $F = 2.72489$, $G = 0.227836$.

Spherical cutoffs for the short-range forces were used. The non-Coulombic pair forces were cut off at 14 Å, and the three-body forces, at 6 Å. For the Coulombic interactions, Ewald lattice sums[53] were used.

The equations of motion were integrated using the velocity version[54] of the Verlet[55] integrator with a time step of 1.5 fs. The water molecules were kept rigid using an accelerated version[56] of the RATTLE[57] version of the SHAKE[58] method of constraint dynamics.

The simulations were performed in various ensembles. In the NVT and NPT ensembles, the temperature was kept at an average of 298 K using the extended system method of Nosé and Hoover.[59,60] In the NPT ensemble, the pressure was kept at an average of 0 Pa using the method of Hoover.[60]

Four sets of simulations were performed, following the strategy discussed in the Methodology section.

(1) A 900-ps "direct simulation" in the NPT ensemble without any ion−water distance constraints was performed to determine the radial distribution function, running coordination number (Figure 2), "the rate constant from direct simulation", and "the exchange mechanism from direct simulation". The potential of mean force $W(r)$ (Figure 3) was obtained from the radial distribution function using eq 2. The PMF obtained in this way is of poor quality close to the maximum because of the rather rare occurrence of a water molecule being located between the first and second hydration shells.

(2) A set of 15 simulations, each 150 ps long, with one ion−water distance constrained between 2.3 and 3.4 Å (as discussed in the Methodology section) were performed to improve the PMF close to the maximum (Figure 3). These simulations were performed in the NVT ensemble with the volume set to the average volume of the direct simulation in the NPT ensemble. In each of these simulations, the force on the constraint was recorded and averaged to give the mean force at the particular distance (cf. section 2.1). The mean force versus distance curve was integrated to give the PMF force. The PMF obtained in this way replaces the direct-simulation PMF around the maximum.

(3) Initial configurations for the reactive flux calculation were generated using a set of five simulations in the NVT ensemble, each 1.5 ns long, with the Li^+−water distance constrained to

$r^{\ddagger} = 2.70$ Å. The system configuration was stored every 3 ps, giving a total of 2500 stored configurations. These simulations were also used to compute the time-dependent friction used in the calculations of the transmission coefficient from the Grote−Hynes theory.

(4) These 2500 generated configurations were used as starting points for the reactive flux method. The Li^+−water constraints were removed, and new velocities for the ion and water molecule were sampled from a Boltzmann distribution. Each configuration was followed 1.5 ps forward and 1.5 ps backward in time. These simulations were all performed in the NVE ensemble to prevent any effect that the thermostat may have on the dynamics of the particles, even though the expected effect on the individual trajectories is small. Note that the initial configurations are still in the (constrained) canonical ensemble.

4. Results and Discussion

4.1. Structure. The Li^+−water center-of-mass radial distribution function (Figure 2) obtained from the direct simulation shows a peak at 2.02 Å for the first hydration shell and a peak centered around 4.19 Å for the second hydration shell. Integration of the first peak up to the first minimum at approximately 2.7 Å gives an average coordination number of 4.02 water molecules. The Li^+−water oxygen radial distribution function (not shown) shows the first peak at 1.96 Å. This agrees well with previous ab initio-level results.[11,34−36] The results also agree fairly well with experiment (Table 1). It must be pointed out, however, that such comparisons are seldom straightforward. For example, the experimental results quoted here refer to quite concentrated solutions (and suggest a significant concentration dependence of the coordination number at these high concentrations) whereas most of the simulation studies were made at considerably lower concentrations, with or without counterions included. Systematic errors in both the experimental and computational studies add to the difficulty of comparison, with the choice of force field perhaps being the most crucial aspect of the simulation studies.

4.2. Exchange Rate. The potential of mean force, $W(r)$, obtained from the radial distribution function using eq 2 and the centrifugally averaged potential of mean force, $W_{\mathrm{eff}}(r)$, are shown in Figure 3. The dissociation barrier is $\sim 5\ k_B T$ ($\sim$12.5 kJ/mol), which can be compared to the activation barrier of $\sim 4\ k_B T$ ($\sim$10 kJ/mol) for the larger ion Na^+(aq) obtained by Rey and Hynes.[14] Figure 4 shows the PMF as obtained from $g(r)$ in the region between the first and second hydration shells, together with the mean force and the PMF obtained from the mean force. The PMF obtained from $g(r)$ is seen to be considerably more noisy, which is why the PMF from the mean force was used for this region in the subsequent analysis. The resulting k^{TST} value using eq 1 is 63.2 ns^{-1}.

The transmission coefficient as obtained from the plateau value of the normalized reactive flux (Figure 5) is 0.14 ± 0.02; this substantial recrossing correction to TST is even lower than the value obtained for Na^+(aq).[14] The error in the transmission coefficient was estimated as the 95% confidence interval of the mean when dividing the data into five independent blocks.[61] The resulting rate constant κk^{TST} is 8.9 ± 1.3 ns^{-1}.

The exchange rate constant from the direct simulation obtained using eq 4 is 14 ± 8 ns^{-1}, where the error was estimated as above.

The transmission coefficient was also obtained from Grote−Hynes theory, eq 5, giving a κ_{GH} of 0.415, resulting in a rate constant $\kappa_{\mathrm{GH}} k^{\mathrm{TST}}$ equal to 26.2 ns^{-1}. The exchange rate constants obtained with the different methods are summarized in Table 3. Inverting the rate constant gives the mean residence time for a solvent molecule in the first hydration shell and is equal to 112 ± 16 ps from the reactive flux method; this is in fair agreement with experiment (Table 2). The results from the direct simulation (71 ± 41 ps, cf. Table 3) and the reactive flux method are consistent. However, the result obtained using Grote−Hynes theory is clearly too large; this unusual failure is consistent with the results previously obtained for Na^+(aq)[14] and, as was the case there, arises from recrossing trajectories that make large excursions from $r^{\ddagger}$, in violation of the assumption of the theory.

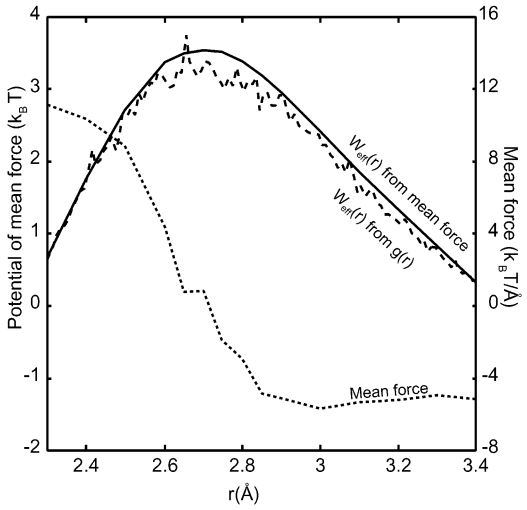

Figure 4. Mean force (···) and effective potential of mean force (—, - - -). The solid line was obtained by integrating the mean force, and the dashed line, from $g(r)$.

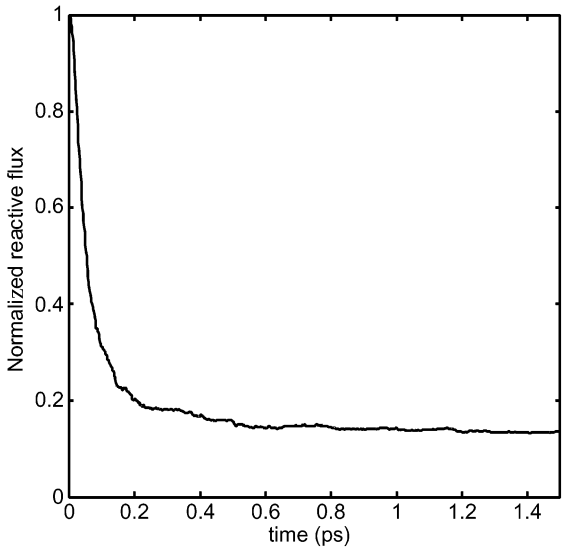

Figure 5. Normalized reactive flux.

TABLE 3: Resulting Exchange Rates Using Different Methods

method	κ	$k = \kappa k^{\mathrm{TST}}$
direct simulation		14 ± 8 ns^{-1}
reactive flux	0.14 ± 0.02	8.9 ± 1.3 ns^{-1}
Grote−Hynes theory	0.42	27 ns^{-1}

4.3. Exchange Mechanisms. Figure 6 shows some of the idealized mechanisms (A, I, D) for water exchange around the lithium ion. The percentages indicated there for various events are those expected on the basis of various simple considerations discussed below. The I_a and I_d mechanisms can be thought of as resembling the I mechanism with respectively shorter or

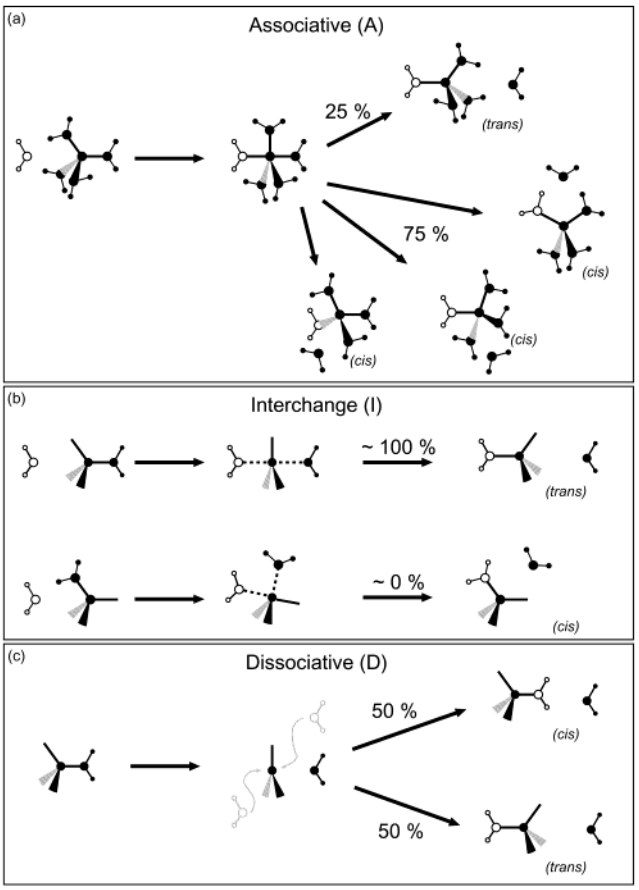

Figure 6. Schematic pictures of exchange mechanism classifications and idealized stereochemical correlation. The incoming water molecule is outlined in the pictures for clarity. The percentages listed are those expected on the basis of simple considerations according to the discussion in the text. (a) Associative. (b) Interchange. (c) Dissociative.

longer distances between the ion and exchanging water molecules, thereby also resembling the A and D mechanisms (Figure 1). The four water molecules normally surrounding the lithium ion usually form a tetrahedron. In an idealized associative mechanism (Figure 6a), a trigonal bipyramid is formed where the incoming water molecule will form 90° and 180° water−ion−water angles with the other first-shell water molecules. If the outgoing water molecule is approximately opposite to the incoming water molecule, then the exchange mechanism is of the trans type (see Introduction) or, alternately stated, of the "backside-attack" type, leading to the well-known Walden inversion.[41] If, however, the outgoing water molecule is one of the three 90° molecules, then the mechanism is of the cis type (i.e., of the "frontside-attack" type).

In an idealized dissociative exchange mechanism, a trigonal-planar coordination geometry is formed, as shown in Figure 6c. The incoming water molecule can then enter either on the same side as (cis) or on the opposite side (trans) of the outgoing water molecule.

The idealized interchange mechanism is shown in Figure 6b. Because of steric hindrance between the entering and leaving water molecules in a cis-type interchange mechanism, the trans mechanism ought to be more likely for a metal ion with no repulsion between the ligands and *d* electrons, such as Li^+. Here, we include all types of short-range repulsive interactions in the concept of steric hindrance. Substitution mechanisms for tetrahedrally coordinated metal ions are not studied as much as those for octahedral or square-planar complexes, but the resemblance to the substitution mechanisms on a saturated carbon atom[41] is apparent.

TABLE 4: Number of Exchanges of Different Types Based on a Stereochemical Analysis of the Various Exchange Events Occurring during the Simulations[a]

	direct simulation			reactive flux		
	cis	trans	total	cis	trans	total
A	10	9	19	78	69	147
I_a	5	14	19	41	93	134
I	2	5	7	9	15	24
I_d	0	1	1	3	2	5
D	0	0	0	0	0	0
other			2			19
total	17	29	48	131	179	329

[a] See Introduction for the definitions of the A, I_a ... notation and section 4.3 for the definition of the cis, trans notation.

Table 4 shows the number of exchanges of the different types, obtained as described in the Methodology section. The relative occurrences of exchanges of each type are seen to be very similar in the reactive flux and the direct simulation methods, although the former method allows for greatly improved sampling and statistics.

The most common mechanism found is of the associative (A) type, with the associative interchange (I_a) almost as common. Together, these two occur in about 80% of the cases. Exchanges of interchange type (I) and of dissociative interchange type (I_d) occur in approximately 10 and 2% of the cases, respectively. No exchanges of the dissociative (D) type were found. It is interesting that experimentally it has been found that the exchanges around the Be^{2+}(aq) ion, which is also tetrahedrally coordinated and even smaller than Li^+, are clearly associative.[62]

As shown in Figure 6a, when a trigonal bipyramid is formed in the associative mechanism (A), there are four possible ways for a water molecule to leave. If the higher-coordinated intermediate would live for a long enough time for the solvent memory (e.g., the second-shell coordinate pattern induced by the entrance of the fifth member into the Li^+ first coordination shell) to vanish and for the initial momentum to spread among the molecules in the first solvation shell (as well as to molecules in the second shell), then there would be no preferences concerning which of the water molecules will leave. This would lead to the cis exchange being 3 times as common as the trans exchange, as indicated by the idealized percentages in Figure 6a. Figure 7 follows two water molecules during the exchange process occurring in the simulation. For this particular event, a rather long-lived (0.6−0.7 ps) "intermediate" finally leading to cis exchange is observed. However, the exchange intermediates, or activated complexes in our MD simulation, are usually much more short-lived than the one in Figure 7. As shown in Table 4 for the associative mechanism (A), there is an "nonstatistical" bias in favor of trans exchanges; close to 50% of the exchanges are of the trans type.

Turning to the I and I_a mechanisms, one idealized image (especially for the former) would be based on the organic S_N2 Walden inversion[41] in which the leaving water is trans to the attacking water. (An example of a trans-type I_a mechanism occurring in the simulations is shown in Figure 8.) This image is the basis of the idealized expected percentages for trans (∼100) and cis (∼0) in Figure 6b. Table 4 shows instead that for I events the observed bias in favor of trans over cis is much less than the idealized expectation. Furthermore, the Table 4 entries for the more numerous I_a-type exchanges also show that

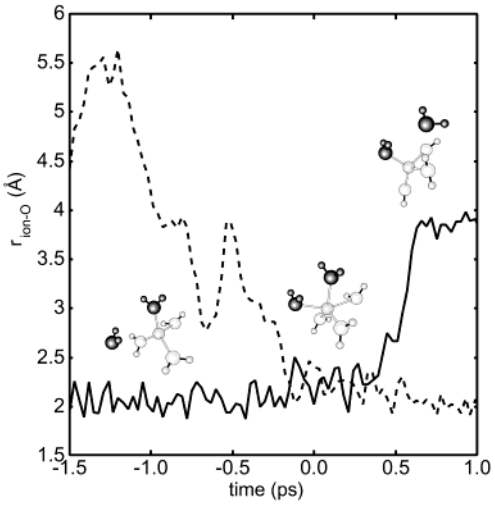

Figure 7. Associative cis mechanism. The solid line shows the distance between the ion and the leaving water molecule, and the dashed line the distance between the ion and the entering water molecule. The entering and leaving water molecules are shown in the picture.

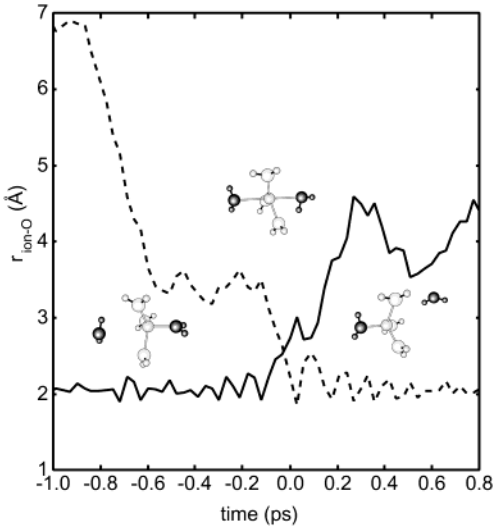

Figure 8. Associative interchange, trans mechanism. Same notation as in Figure 7.

trans is favored, but to an extent rather less than the idealized image of Figure 6b. For the I (and I_a) exchanges, a possible source for departure from the idealized image is that the steric hindrance is very likely less for electrostatically bound water around Li^+ than, for instance, covalently bound groups around carbon.[41] Moreover, the recrossings in the transition-state region also lead to an apparent prolonged lifetime of the "activated complex", which would spread the initial momentum of the attacking water over the first (and second) solvation shell molecules rather than transfer it directly to the trans leaving water. It should also be noted that, since I_a exchanges are in a sense a borderline between A and I exchanges (cf. Figure 4), the trans/cis ratio found for I_a (Table 4) could also be considered using the idealized image we used for A exchanges several paragraphs above; in this alternate perspective, there is, as was the case for A, a much higher trans occurrence than expected from the idealized image.

The number of I_d exchanges are too few to allow a more detailed analysis, but they indicate that the idealized model picture (Figure 6c) is correct, assuming that the I_d mechanism resembles both the I and D mechanisms.

The observed differences in the exchange stereochemistry between the idealized images and the actual simulation results pointed out above may be explained by the fact that the mechanism classes as defined here strictly consider the ion−water distances of only the two exchanging water molecules (i.e., the lifetimes of the intermediates/activated complexes are not taken into account). Moreover, the idealized model pictures include only the positions of the first solvation shell molecules plus the exchanging water molecules and basically ignore the momentum of the first solvation shell molecules as well as the positions and momentum of the second shell and bulk water molecules. In the case of an associative exchange, for example, the steric hindrance should be virtually unimportant with respect to the choice of a cis or trans leaving group since here both the entering and leaving molecule are already in the first hydration shell. The favoring of the trans mechanism for the A and I_a exchanges (in considerable excess of the expectations based on the idealized image of complete loss of memory in both momentum and second solvation shell configurations) may be partially explained, at least for the *very* short-lived complexes, by taking the momentum of the molecules in the first solvation shell into account. If the attacking water molecule has momentum straight toward the ion, then the water molecule most likely to leave is the one on the opposite side, corresponding to the trans mechanism, from pure conservation-of-momentum considerations. It is not clear, however, whether such events are significantly more common than events where the momentum of the attacking water molecule is directed more orthogonally to the ion−first-shell water distance vector; the latter would be expected to favor an exchange mechanism of the cis type on the grounds of conservation of momentum of the two exchanging molecules. However, if in fact the latter effect is small, then the explanation must be sought in, for example, aspects of the configurations of the second solvation shell waters. This is a topic for further research.

As has been observed earlier in MD simulations[6] using other potentials, it is rather common that the exchange mechanism cannot be completely classified in terms of the A, I_a ... mechanisms. Such examples are, for instance, exchanges where two or more water molecules exchange at the same time, leading to a coordination number between 4 and 6 during the exchange. Exchanges of this type are collected in the "other" section in Table 4 but are not of frequent occurrence. Recrossings at the transition state as observed by Rey and Hynes[4] for Na^+(aq) are also common and are reflected in the low transmission coefficient obtained from the reactive flux method. Recrossings are, however, *not* collected in the "other" section, but instead, the distance at the last crossing point is used. These factors make the application of more automated procedures for a detailed exchange-mechanism analysis difficult and explain why the visual approach is very valuable and was used here.

5. Concluding Remarks

The exchange rate of water molecules around Li^+(aq) has been determined from MD simulations both directly and by employing the reactive flux method. The results are in fair agreement with each other and with experiment. The Grote−Hynes theory overestimates the transmission coefficient because of a violation of its assumptions. The mechanisms of the exchange have been studied in detail, with most exchanges being of an associative or associative interchange type. The stereochemistry of the exchanges reveals a complex picture that is in part explainable by idealized model pictures, but departures from these pictures are observed. For the associative exchanges, the

trans-type mechanism is more common than predicted. Also, trans-type exchanges for the associative interchange and interchange-type mechanisms are clearly favored by the steric hindrance considerations, but the favoring is less than predicted by the idealized model pictures. These observations indicate that a complete understanding of the exchange features will require attention not only to the configurations of the first hydration shell of the ion but also to dynamical and configurational issues related to momentum transfer and the second hydration shell.

Acknowledgment. D.S. and K.H. gratefully acknowledge the Swedish Research Council (VR) and the National Graduate School in Scientific Computing (NGSSC) for financial support. R.R. gratefully acknowledges support from MCYT project BFM2001-2077. This work was supported in part (J.T.H.) by the CNRS and NSF grant CHE-0108314. We acknowledge support from the European Commission within the framework of the RTN contract no. HPRN-CT-2000-19.

References and Notes

(1) Friedman, H. L. *Chem. Scr.* **1985**, *25*, 42.
(2) DuCommun, Y.; Merbach, A. E. In *Studies in Inorganic Chemistry 7: Inorganic High-Pressure Chemistry, Kinetics and Measurements*; van Eldik, R., Ed.; Elsevier: Amsterdam, 1986.
(3) Ohtaki, H.; Radnai, T. *Chem. Rev.* **1993**, *93*, 1157.
(4) Rey, R.; Hynes, J. T. *J. Phys. Condens. Matter* **1996**, *8*, 9411.
(5) Kowall, T.; Foglia, F.; Helm, L.; Merbach, A. E. *Chem.—Eur. J.* **1996**, *2*, 285.
(6) Spångberg, D.; Wojcik, M.; Hermansson, K. *Chem. Phys. Lett.* **1997**, *276*, 114.
(7) Hermansson, K.; Wojcik, M. *J. Phys. Chem. B* **1998**, *102*, 6089.
(8) Åkesson, R.; Pettersson, L. G. M.; Sandström, M.; Wahlgren, U. *J. Am. Chem. Soc.* **1994**, *116*, 8705.
(9) Hartmann, M.; Clark, T.; van Eldik, R. *J. Am. Chem. Soc.* **1997**, *119*, 7843.
(10) Rotzinger, F. P. *J. Am. Chem. Soc.* **1997**, *119*, 5230.
(11) Lyubartsev, A. P.; Laasonen, K.; Laaksonen, A. *J. Chem. Phys.* **2001**, *114*, 3120.
(12) Impey, R. W.; Madden, P. A.; McDonald, I. R. *J. Phys. Chem.* **1983**, *87*, 5071.
(13) Szász, G. I.; Heinzinger, K. *J. Chem. Phys.* **1983**, *79*, 3467.
(14) Rey, R.; Hynes, J. T. *J. Phys. Chem.* **1996**, *100*, 5611.
(15) Kowall, T.; Foglia, F.; Helm, L.; Merbach, A. E. *J. Am. Chem. Soc.* **1995**, *117*, 3790.
(16) Obst, S.; Bradaczek, H. *J. Phys. Chem.* **1996**, *100*, 15677.
(17) Lee, S. H.; Rasaiah, J. C. *J. Chem. Phys.* **1994**, *101*, 6964.
(18) Lee, S. H.; Rasaiah, J. C. *J. Phys. Chem.* **1996**, *100*, 1420.
(19) Koneshan, S.; Rasaiah, J. C.; Lynden-Bell, R. M.; Lee, S. H. *J. Phys. Chem. B* **1998**, *102*, 4193.
(20) Heinzinger, K.; Vogel, P. C. *Z. Naturforsch.* **1974**, *29*, 1164.
(21) Szász, G. I.; Heinzinger, K.; Riede, W. O. *Z. Naturforsch.* **1981**, *36*, 1067.
(22) Bopp, P.; Okada, I.; Ohtaki, H.; Heinzinger, K. *Z. Naturforsch.* **1985**, *40*, 116.
(23) Cieplak, P.; Kollman, P. *J. Chem. Phys.* **1990**, *92*, 6761.
(24) Åqvist, J. *J. Phys. Chem.* **1990**, *94*, 8021.
(25) Floris, F. M.; Persico, M.; Tani, A.; Tomasi, J. *Chem. Phys.* **1995**, *195*, 2078.
(26) Periole, X.; Allouche, D.; Daudey, J. P.; Sanejouand, Y. H. *J. Phys. Chem. B* **1997**, *101*, 5018.
(27) Periole, X.; Allouche, D.; Ramírez-Solís, A.; Ortega-Blake, I.; Daudey, J. P.; Sanejouand, Y. H. *J. Phys. Chem. B* **1998**, *102*, 8579.
(28) Bounds, D. G. *Mol. Phys.* **1985**, *54*, 1335.
(29) Pettitt, B. M.; Rossky, P. J. *J. Chem. Phys.* **1986**, *84*, 5836.
(30) Floris, F. M.; Persico, M.; Tani, A.; Tomasi, J. *Chem. Phys. Lett.* **1992**, *199*, 518.
(31) Yamaguchi, T.; Spohr, E.; Pálinkas, G.; Heinzinger, K.; Probst, M. M.; Ohtaki, H. *Z. Naturforsch., A: Phys. Sci.* **1986**, *41*, 1175.
(32) Probst, M. M.; Spohr, E.; Heinzinger, K. *Chem. Phys. Lett.* **1989**, *161*, 405.
(33) Lauenstein, A.; Hermansson, K.; Lindgren, J.; Probst, M.; Bopp, P. A. *Int. J. Quantum Chem.* **2000**, *80*, 892.
(34) Tongraar, A.; Liedl, K. R.; Rode, B. M. *Chem. Phys. Lett.* **1998**, *286*, 56.
(35) Feller, D.; Glendening, E. D.; Kendall, R. A.; Peterson, K. A. *J. Chem. Phys.* **1994**, *100*, 4981.
(36) Feller, D.; Glendening, E. D.; Woon, D. E.; Feyereisen, M. W. *J. Chem. Phys.* **1995**, *103*, 3526.
(37) Burgess, J. *Ions in Solution*; Ellis Horwood Ltd.: West Sussex, England, 1988.
(38) Salmon, P. S.; Howells, W. S.; Mills, R. *J. Phys. C: Solid State Phys.* **1987**, *20*, 5727.
(39) Langford, C. H.; Gray, H. B. *Ligand Substitution Processes*; W. A. Benjamin: New York, 1966.
(40) Basolo, F.; Pearson, R. G. *Mechanisms of Inorganic Reactions*; John Wiley & Sons: New York, 1958.
(41) Ingold, C. K. *Structure and Mechanism in Organic Chemistry*, 2nd ed; Cornell University Press: Ithaca, NY, 1969.
(42) Lincoln, S. F.; Merbach, A. E. *Adv. Inorg. Chem.* **1995**, *42*, 1.
(43) Helm, L.; Merbach, A. E. *Coord. Chem. Rev.* **1999**, *187*, 151.
(44) Spångberg, D.; Hermansson, K. To be submitted for publication. Details about the potentials can be obtained from D.S. (daniels@mkem.uu.se).
(45) Cicotti, G.; Ferrario, M.; Hynes, J. T.; Kapral, R. *Chem. Phys. Lett.* **1989**, *156*, 472.
(46) Cicotti, G.; Ferrario, M.; Hynes, J. T.; Kapral, R. *Chem. Phys.* **1989**, *129*, 241.
(47) Guàrdia, E.; Rey, R.; Padró, J. A. *Chem. Phys.* **1991**, *155*, 187.
(48) Chandler, D. *J. Chem. Phys.* **1978**, *68*, 2959.
(49) Carter, E. A.; Cicotti, G.; Hynes, J. T.; Kapral, R. *Chem. Phys. Lett.* **1989**, *156*, 742.
(50) Grote, R. F.; Hynes, J. T. *J. Chem. Phys.* **1980**, *73*, 2715.
(51) Spångberg, D. *Ymol*; 1998. A molecular visualization and animation program.
(52) Berendsen, H. J. C.; Grigera, J. R.; Straatsma, T. P. *J. Phys. Chem.* **1987**, *91*, 6269.
(53) Ewald, P. *Ann. Phys.* **1921**, *64*, 253.
(54) Swope, W. C.; Andersen, H. C.; Berens, P. H.; Wilson, K. R. *J. Chem. Phys.* **1982**, *76*, 637.
(55) Verlet, L. *Phys. Rev.* **1967**, *159*, 98.
(56) Barth, E.; Kuczera, K.; Leimkuhler, B. J.; Skeel, R. D. *J. Comput. Chem.* **1995**, *16*, 1192.
(57) Andersen, H. C. *J. Comput. Phys.* **1983**, *52*, 24.
(58) Ryckaert, J. P.; Ciccotti, G.; Berendsen, H. J. C. *J. Comput. Phys.* **1977**, *23*, 327.
(59) Nosé, S. *Mol. Phys.* **1984**, *52*, 255.
(60) Hoover, W. G. *Phys Rev. A* **1985**, *31*, 1695.
(61) Rey, R. *J. Chem. Phys.* **1996**, *104*, 1966.
(62) Pittet, P. A.; Elbaze, G.; Helm, L.; Merbach, A. E. *Inorg. Chem.* **1990**, *29*, 1936.
(63) Cartailler, T.; Kunz, W.; Turq, P.; Bellisent-Funel, M.-C. *J. Phys.: Condens. Matter* **1991**, *3*, 9511.
(64) Musinu, A.; Paschina, G.; Piccaluga, G.; Magini, M. *J. Chem. Phys.* **1984**, *80*, 2772.
(65) Newsome, J. R.; Neilson, G. W.; Enderby, J. E. *J. Phys. C: Solid State Phys.* **1980**, *13*, L923.